

Engineering exotic phases for topologically-protected quantum computation by emulating quantum dimer models

A. Fabricio Albuquerque,^{1,2} Helmut G. Katzgraber,¹ Matthias Troyer,¹ and Gianni Blatter¹

¹*Theoretische Physik, ETH Zurich, 8093 Zurich, Switzerland*

²*School of Physics, The University of New South Wales, Sydney, New South Wales 2052, Australia*

(Dated: October 24, 2018)

We use a nonperturbative extended contractor renormalization (ENCORE) method for engineering quantum devices for the implementation of topologically protected quantum bits described by an effective quantum dimer model on the triangular lattice. By tuning the couplings of the device, topological protection might be achieved if the ratio between effective two-dimer interactions and flip amplitudes lies in the liquid phase of the phase diagram of the quantum dimer model. For a proposal based on a quantum Josephson junction array [L. B. Ioffe *et al.*, *Nature (London)* **415**, 503 (2002)] our results show that optimal operational temperatures below 1 mK can only be obtained if extra interactions and dimer flips, which are not present in the standard quantum dimer model and involve three or four dimers, are included. It is unclear if these extra terms in the quantum dimer Hamiltonian destroy the liquid phase needed for quantum computation. Minimizing the effects of multi-dimer terms would require energy scales in the nano-Kelvin regime. An alternative implementation based on cold atomic or molecular gases loaded into optical lattices is also discussed, and it is shown that the small energy scales involved—implying long operational times—make such a device impractical. Given the many orders of magnitude between bare couplings in devices, and the topological gap, the realization of topological phases in quantum devices requires careful engineering and large bare interaction scales.

PACS numbers: 03.67.Pp,74.81.Fa,75.10.Jm

I. INTRODUCTION

Systems characterized by topological quantum order (TQO) have a degenerate ground state, which is not associated with any broken symmetry, i.e., the different degenerate ground states are indistinguishable under the action of any local operator.¹ Instead, they can only be distinguished via global operators intimately related to their topological properties. TQO does not fit into Landau’s paradigm for ordered phases of matter,² which makes it intrinsically interesting. Furthermore, this robustness against local perturbations characteristic of systems exhibiting TQO can be used to implement a fault-tolerant quantum computer.³

Within this approach, robust storage devices for quantum states (“protected memory qubits”) can be built from Abelian topological quantum states, whereas topologically-protected computations (“protected gates”) can be implemented using non-Abelian states.³ Given the enormous challenges involved in building conventional quantum computers caused by the decoherence inherent to quantum-mechanical systems, the alternative approach exploiting topological order has attracted considerable interest recently because local operators (i.e., noise) do not disturb the topological phase.

One promising class of systems exhibiting TQO are fractional quantum Hall systems with filling factors $\nu = 5/2$ and $\nu = 12/5$ which are conjectured to exhibit non-Abelian anyonic excitations.⁴ Unfortunately, despite some evidence,⁵ the existence of anyons in these systems remains to be confirmed experimentally. On the other hand, a number of interesting lattice models is

known to exhibit TQO. Among these are quantum dimer models (QDM) (Refs. 6,7,8,9) spin models, and Hubbard models with generalized interactions defined on Kagome lattices,^{10,11,12,13} toric,³ and color¹⁴ codes, as well as Kitaev’s honeycomb anisotropic spin model.¹⁵ In general, these lattice models incorporate unrealistic elements such as artificially-constrained degrees of freedom or nontrivial interactions and thus experimental realizations remain elusive. Therefore, we are interested in engineering topologically-ordered phases by *emulating* lattice models using highly manipulable quantum *tool-boxes*, such as Josephson junction arrays⁸ and cold atomic¹⁶ or molecular^{17,18} gases loaded into optical lattices. However, as promising as these approaches might seem, the challenges imposed to the engineering of such emulators are huge, requiring special attention to the *design* of such devices and a careful analysis of the involved energy scales as well as the possible existence of extra terms in the emulated Hamiltonian.

Having these issues in mind, we use a *nonperturbative* algorithm, extended contractor renormalization (ENCORE) (Ref. 19) an extended version of the Contractor Renormalization (CORE) technique^{20,21} to design exotic phases to build topological quantum computers as well as to propose controllable experiments to investigate TQO. We consider an emulator for the QDM on the triangular lattice based on an array of quantum Josephson junctions.⁸ This system is a good candidate for the implementation of a topologically-protected qubit for two reasons: First, quantum dimer models are among the best understood systems exhibiting TQO and the presence of a topological phase has been unequivocally established in

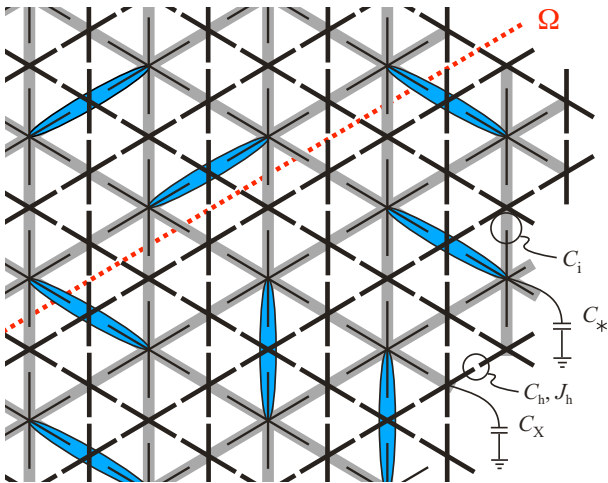


FIG. 1: (Color online) Array of Josephson junctions used to emulate the quantum dimer model on the triangular lattice. The array is formed by X-shaped superconducting islands (thick black lines), which form a Kagome lattice and normal-state star-shaped islands (thin black lines) placed at the center of every hexagon of the Kagome lattice. The shaded lines are guides to the eye to emphasize the underlying triangular lattice of the effective QDM. Cooper pairs hop between nearest-neighbor X-shaped islands with an amplitude given by the Josephson current J_h . A large ratio between the capacitances C_i and C_h defines a sizable on-hexagon repulsion E_{hex} to emulate the hard-core dimer constraint. The dimers are represented by ellipses sitting on one of the six links of a given star-shaped island. The parity of the dimer count along a reference line Ω (dotted line) is invariant under the dimer flips in the Hamiltonian [Eq. (1)].

The energetic cost for placing two bosons around the same hexagon E_{hex} defines the basic energy scale of the array. It should not be confused with the on-site repulsion between two Cooper pairs sitting on the same X-shaped island. The parity of the dimer count along the reference line Ω (dotted line in Fig. 1) is invariant under dimer flips (local perturbations) in the Hamiltonian [see Eq. (1)] and allows for the determination of the topological sectors necessary to define a qubit state.

C. Emulator Based on Cold Atomic/Molecular Gases

We also consider an implementation of the QDM based on cold atomic/molecular gases loaded into a Kagome optical lattice, which can in principle be created by using three laser beams,²⁶ with the following Hamiltonian:

$$\mathcal{H} = \frac{U}{2} \sum_i n_i(1 - n_i) + \frac{E_{\square}}{2} \sum_{\square} n_{\square}(n_{\square} - 1) - J \sum_{\langle i,j \rangle} (b_i^{\dagger} b_j + b_j^{\dagger} b_i). \quad (4)$$

Here $n_i = b_i^{\dagger} b_i$ is the bosonic number operator at the site i of the Kagome lattice, U is a repulsion between two bosons sitting on the same site and J is the hopping amplitude between nearest-neighbor sites $\langle i, j \rangle$ in the Kagome lattice. E_{\square} is the energy required for placing two bosons on *different* sites around the same hexagon in the Kagome lattice and enforces the hard-core dimer condition. n_{\square} is the number of bosons sitting around a given hexagon. Due to the short-ranged interactions between cold atomic gases, the engineering of interaction terms as in Eq. (4) would likely be a highly nontrivial task. One possible solution to this problem is to use polar molecules^{17,18} whose permanent dipole moment permits long-range interactions.

III. EFFECTIVE HAMILTONIANS FROM THE ENCORE METHOD

The CORE method was originally introduced by Morningstar and Weinstein^{20,21} and since then has been successfully applied to different problems in strongly correlated systems.^{27,28,29,30,31,32,33} For our application we use an extended version, ENCORE, suitable for constrained models, such as the quantum dimer model.¹⁹

The fundamental idea behind CORE and ENCORE is to derive an effective model describing the low-energy physics of a lattice Hamiltonian by reducing the number of degrees of freedom. The usefulness of the method relies on a fast decay of the effective interactions for the specific effective model, something which needs to be verified for each case. A large amount of physical intuition is required to obtain physically sound results, which is one reason why CORE has not found a more widespread use to date.

The effective Hamiltonian obtained with ENCORE generally includes arbitrarily-ranged terms. Large couplings associated with long-range terms indicate that the restricted subspace does not accurately describe the low-energy behavior of the original model. However, if we are interested in engineering an emulation of a certain Hamiltonian, the aforementioned problems are irrelevant because in this case the effective model and the restricted Hilbert space are known *a priori*. If the ENCORE method fails we simply conclude that emulation is not possible.

The breakdown of the mapping is also signaled by the appearance of “intruder” states in the low-lying spectrum. These are states with negligible overlap with any of the desired low-energy states. Since both aforementioned effects are correlated,¹⁹ we avoid the adoption of an arbitrarily-defined threshold value for the long-range interactions and we define the breakdown of the mapping onto a QDM as the point where a first intruder state appears in the device’s low-energy spectrum.

Since our primary goal in the present paper is to verify the feasibility of a fault-tolerant quantum bit engineered from a system with a topologically-ordered phase, the

device's parameters must be tuned in order to ensure that the emulated model has couplings known to correspond to a quantum dimer liquid phase. In addition, a careful analysis of the involved energy scales is necessary in order to avoid technological limitations.

IV. EMULATING QUANTUM DIMER MODELS USING JOSEPHSON JUNCTION ARRAYS

The array of Josephson junctions discussed in Sec. II B can be described by the following generalized Bose-Hubbard Hamiltonian

$$\mathcal{H} = \frac{1}{2} \sum_{j,k} n_j \hat{C}_{j,k}^{-1} n_k - J_h \sum_{\langle j,k \rangle} (b_j^\dagger b_k + b_k^\dagger b_j). \quad (5)$$

The positions of the X-shaped islands in the array are denoted by the indices j and k . $\langle j,k \rangle$ represent nearest neighbor (NN) sites in the Kagome lattice. $n_j = b_j^\dagger b_j$ is the bosonic occupation number at site \vec{r}_j , J_h is the Josephson current between two X-shaped islands.

\hat{C}^{-1} is obtained by numerically inverting the capacitance matrix \hat{C} of the array. The matrix elements connecting two X-shaped islands in this matrix are given by

$$\hat{C}_{j,k} = [C_X + \mu_j C_i + \nu_j C_h] \delta_{\vec{r}_j, \vec{r}_k} + C_h \delta_{\vec{r}_j, \vec{r}_k + \hat{r}}, \quad (6)$$

where \hat{r} connects NN sites in the Kagome lattice, μ is the number of hexagons a given X-shaped island joins [$\mu = 2$ for full periodic boundary conditions (PBC)] and ν is its number of NN [$\nu = 4$ for PBC].

The normal-state star-shaped islands are only capacitively connected to the X-shaped islands and their only role is to set up the interactions in the Hamiltonian. The inverse \hat{C}^{-1} appearing in the Hamiltonian is sensitive also to these interactions, specified in the following. Star-shaped islands sitting on the sites \vec{R}_α and \vec{R}_β of the underlying triangular lattice contribute with,

$$\hat{C}_{\alpha,\beta} = [C_* + 6C_i] \delta_{\vec{R}_\alpha, \vec{R}_\beta} \quad (7)$$

and the elements connecting X- and star-shaped islands are

$$\hat{C}_{j,\alpha} = C_i \delta_{\vec{r}_j, \vec{r}_\alpha + \vec{s}}, \quad (8)$$

where \vec{s} are the vectors connecting a star-shaped island to the X-shaped islands surrounding it.

The energy E_{hex} to place two dimers on a hexagon can be obtained from certain matrix elements of \hat{C}^{-1} . Quantum fluctuations due to the Josephson coupling J_h reduce this bare value and we thus include them in second order in perturbation theory in our discussions below. To ensure that we are allowed to restrict the calculations to hard-core bosons, we have verified that the on-site repulsion is larger than J_h by a factor of at least 50 for all sets of couplings in the array.

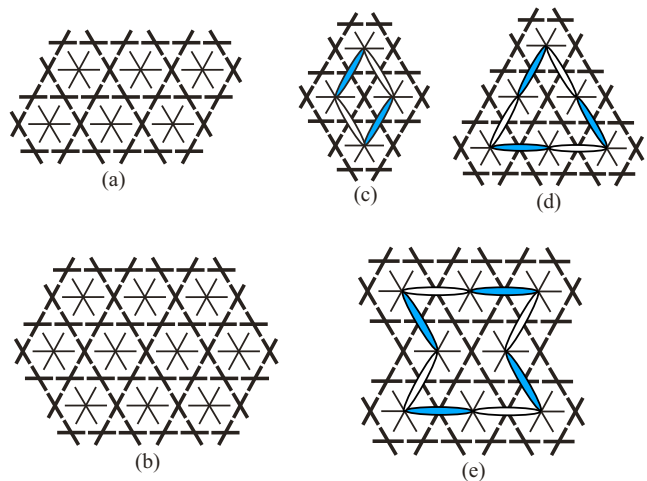


FIG. 2: (Color online) Open-boundary clusters studied: (a) $N \times 2$ ($N = 3$ in the figure) hexagon ladders; (b) ten-hexagon cluster; (c) – (e) special clusters with four, six and eight hexagons, accommodating the lowest-order flip (represented by the associated transition graphs where full dimers flip to open ones) involving two, three, and four dimers, respectively.

Our results are obtained by analyzing the small open-boundary clusters depicted in Fig. 2: ladder-like clusters with $N \times 2$ hexagons ($N = 3, 4,$ and 5), a ten-hexagon cluster (from which most results have been obtained), and three special clusters with four, six, and eight hexagons which accommodate only two distinct dimer configurations each.

Finally we need to take into account experimental limitations. The smallest values for capacitances between two superconducting islands obtainable with current technologies are such that $E^C = 1/2C \sim 1\text{K}$ [see Eq. (3)], higher values of E^C can be obtained for ground capacitances. We set the smallest junction capacitance $C_h = 0.5$, such that $E_h^C = 1$ to set the energy scale, and we restrict our analysis to values of $C_i > C_h$ throughout the rest of this paper. In this way, *assuming* a value of $E_h^C \approx 1\text{K}$, *a priori* taking into account current technological limits, all energies are fortuitously directly given in Kelvin.

A. Dimer Flips

The simplest dimer flip involves two parallel dimers on the same rhombus of the triangular lattice, as illustrated in Fig. 2(c). It involves the creation of a virtual state in which one hexagon is doubly occupied, occurring with an amplitude given in second-order perturbation theory by $t \approx J_h^2/E_{\text{hex}}$. Using ENCORE, we now analyze the amplitude associated with this dimer move for the set of capacitances studied in Ref. 8:

$$\begin{aligned} C_* &= 10, & C_X &= 10, \\ C_i &= 2.0, & C_h &= 0.5. \end{aligned} \quad (9)$$

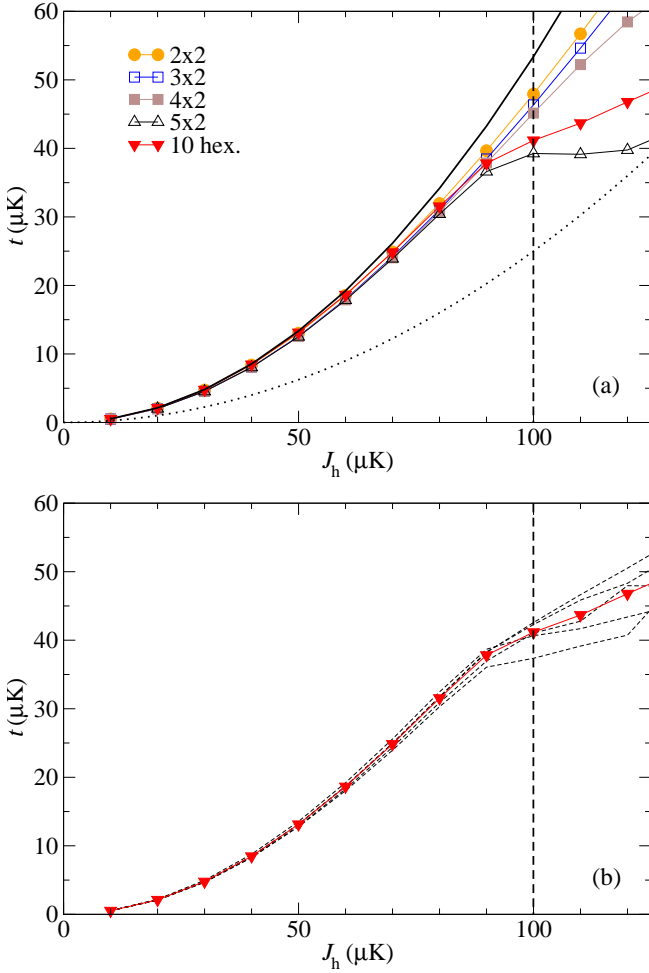


FIG. 3: (Color online) (a) Two-dimer flip amplitude t calculated with ENCORE versus the Josephson current J_h for the clusters depicted in Fig. 2. The parameters of Ref. 8 are used: $C_* = C_X = 10$, $C_i = 2$, and $C_h = 0.5$. Solid lines are only guides to the eye. The vertical dashed line indicates the point where the mapping onto a QDM breaks down (cf. Sec. III). Second-order perturbative results obtained by numerically calculating E_{hex} are indicated by the thick black curve. The dotted curve corresponds to the results obtained by using the expression for E_{hex} derived in Ref. 8. (b) Amplitudes for each of the five nonequivalent two-dimer flips in the ten-hexagon cluster (dashed curves, see main text), compared to their average (downward triangles).

In Fig. 3(a) we show the results for the clusters depicted in Figs. 2(a)–2(c). The absence of substantial finite-size effects confirms that the two-dimer flip is a local process. The different clusters differ only after the point where the mapping onto a QDM breaks down due to the appearance of intruder states (see Sec. III). The results from the ten-hexagon cluster are obtained from an average between the amplitudes for five possible nonequivalent two-dimer flips occurring within slightly different “dimer environments,” the different ways the dimers not participating in the flip are arranged in the cluster.¹⁹ Again, the amplitudes for these individual pro-

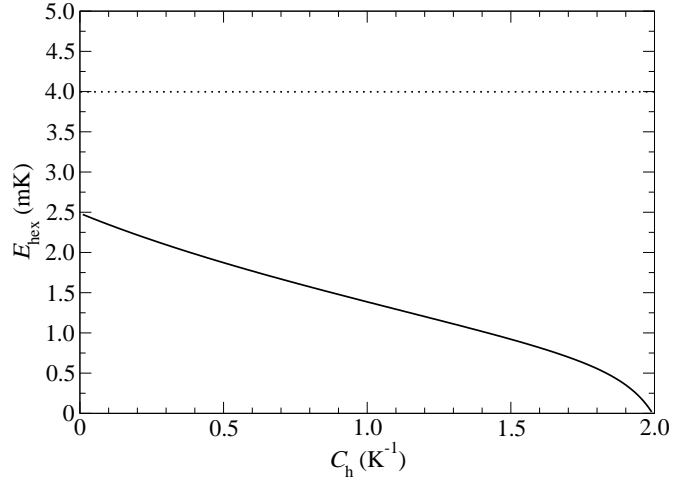


FIG. 4: Numerical second-order perturbative results for the on-hexagon repulsion E_{hex} for the ten-hexagon cluster as a function of the capacitance C_h for $C_* = C_X = 10$ and $C_i = 2$. The horizontal dotted line is $E_{\text{hex}} \sim 0.2(C_i/C_X)^2 E_*^C$, as obtained in Ref. 8.

cesses only deviate slightly from their average until the point where the dimer picture breaks down, as shown in Fig. 3(b).

In Fig. 3(a) we also compare to second-order perturbative data for t , obtained from $t = J_h^2/E_{\text{hex}}$ by numerically calculating E_{hex} for the ten-hexagon cluster (solid line; see Fig. 4), as well as by using the approximation $E_{\text{hex}} \sim 0.2(C_i/C_X)^2 E_*^C$ of Ref. 8. The discrepancy between the two estimates clearly illustrates the nontrivial dependence of E_{hex} on the set of capacitances adopted for the array. Note that E_{hex} vanishes when $C_h = C_i$. Using the accurate estimate for E_{hex} (solid line in Fig. 4), we find reasonable agreement with the ENCORE results, which motivates us to use the perturbative results to guide our optimizations below.

Additional flips involving three and four dimers occurring within third and fourth order in the small parameter J_h with amplitudes t_3 and t_4 respectively, are depicted in Figs. 2(d) and 2(e). Together with the two-dimer flip, these processes are special because they are the lowest-order possible dimer moves in the array: comprising m dimers, they appear as m th order processes in J_h . All other flip terms are strongly suppressed in the limit of small currents J_h . Throughout this paper, we denote the sum of the *absolute values* of the amplitudes for all other dimer moves by Σ , and we use this quantity to gauge the validity of the mapping onto a QDM.

Of particular interest is the flip involving three dimers in a triangular configuration depicted in Fig. 2(d), which has also been found in a recent mean-field mapping by Vernay *et al.*²³ of a spin-orbital model for the compound LiNiO_2 onto a QDM. They found that this extra dimer move considerably to extend the liquid phase, allowing for “extra room” in trying to optimize the couplings in the array. One is tempted to conclude that the four-dimer

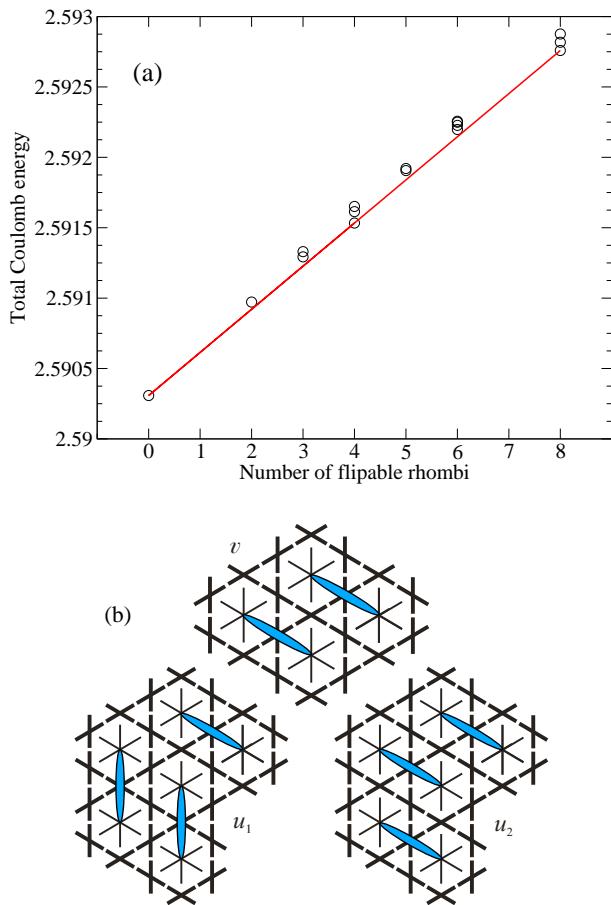


FIG. 5: (Color online) (a) Total Coulomb energy versus number of flipable rhombi (parallel dimers which can flip) for a 4×4 PBC cluster in the limit $J_h = 0$ and with $C_* = C_X = 10$, $C_i = 2$, and $C_h = 0.5$. Deviations from the dominant linear behavior signal the presence of extra interaction terms beyond the one between parallel dimers sitting on the same rhombus with strength v . (b) Interactions present in the limit $J_h = 0$. In addition to the dominant rhombus term v , two further interaction terms involving three dimers with amplitudes u_1 and u_2 have to be included. The deviations from the main contribution in panel (a) can be explained by the presence of these extra terms.

term t_4 has similar effects, and it will be of interest to confirm this numerically.

B. Dimer Interactions

Dimer-dimer interactions have a nontrivial dependence on the particular choice of capacitances in the array and must be tuned in order for the ratio v/t to lie in the liquid phase. To investigate them, we first analyze a 4×4 cluster with PBC in the limit of zero Josephson current ($J_h = 0$) by inverting the capacitance matrix on this cluster. In Fig. 5(a) we show the Coulomb energy as a function of the number of flipable rhombi in each configuration. The total energy scales well with the num-

ber of flipable rhombi, confirming that the interaction between parallel dimers sitting on the same rhombus v is the dominant diagonal term in the emulated dimer Hamiltonian. The deviations from the linear behavior in Fig. 5(a) indicate that other interaction terms are also present. These extra contributions cannot be explained by pairwise interactions, but *all* such deviations are entirely described if we take into account three-dimer interactions with strengths u_1 and u_2 [as shown in Fig. 5(b)].

Understanding the dependence of the interaction strengths on the capacitances of the array is essential for the optimization of the energy scales in the emulated Hamiltonian, and for the minimization of the couplings associated with the three-dimer interactions, the effect of which are unknown. Figure 6 shows the dependence of the couplings v , u_1 , and u_2 on the capacitances³⁴ on the same 4×4 cluster with PBC for $J_h = 0$. The interaction term $v(J_h = 0)$ peaks for small values of C_i and C_X , and $u_1(J_h = 0)$ and $u_2(J_h = 0)$ are appreciable over a significant regime of the parameter space. Decreasing C_* leads to larger values of $u_1(J_h = 0)$ and $u_2(J_h = 0)$ (not shown) but has no significant effects on $v(J_h = 0)$.

To include the effects of nonzero Josephson current J_h on the interactions, we study the ten-hexagon cluster shown in Fig. 2(b) using ENCORE. Due to the small size of the cluster, only four-dimer configurations, out of a total of 14 in this cluster, give nonequivalent diagonal contributions in the effective dimer Hamiltonian. Boundary interactions due to open boundary conditions further complicate the estimates. Without going to larger clusters (which is not possible with current computational resources), we cannot determine the individual terms but only the following combined quantity:

$$v' \equiv v - (u_1 - u_2). \quad (10)$$

which is nevertheless a good estimate for v as we can see by analyzing the 4×4 cluster. As shown in Fig. 6(d), v' underestimates v by typically only 20% for $J_h = 0$ in the region where we have a valid mapping onto the QDM, and these corrections do not change the conclusions drawn below.³⁵

C. Tuning the Ratio v/t

Having discussed the dimer flips and interactions in the array of Josephson junctions, we now analyze the feasibility of the emulation of a topological phase by adjusting the couplings and required energy scales in the emulated QDM to achieve an effective model with couplings in the desired range $0.82 \lesssim v/t \leq 1$.

In Fig. 7 we show the ratio v'/t as a function of the Josephson current J_h for the set $C_* = C_X = 10$, $C_i = 2$ and $C_h = 0.5$ as proposed in Ref. 8 (36). As seen in Fig. 7, the topological phase corresponding to $v'/t < 1$ (marked by dashed horizontal lines) is not reached before the breakdown of the mapping to the QDM. This breakdown, marked by a vertical dashed line is seen both in

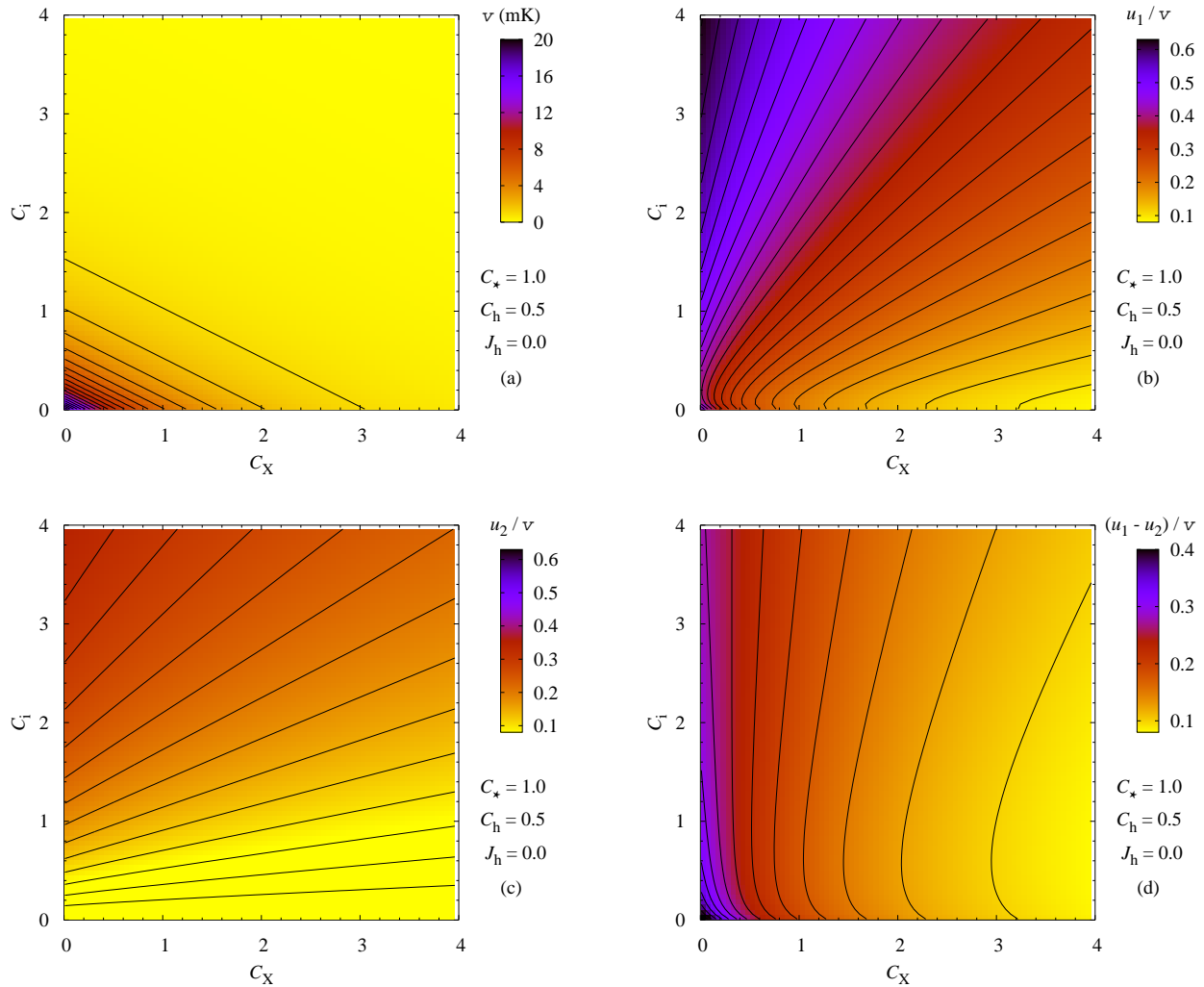


FIG. 6: (Color online) Dependence of the amplitudes v , u_1 and u_2 on the capacitances C_X and C_i , for $C_* = 1$ and $C_h = 0.5$. The results are obtained from the analysis of the 4×4 PBC cluster with $J_h = 0$. Panels (b) and (c) suggest that minimization of u_1 and u_2 is hard to be achieved and panel (d) shows that our results for $v' = v - (u_1 - u_2)$ (our estimate for v for finite values of J_h , see main text) underestimate v by a factor of 40% at most, and typically about 20%.

the appearance of nondimer-like states in the low-lying spectrum as well as by a drastic increase in the summed amplitude for multi-dimer flips (Σ). We conclude that for this value of capacitances no topological phase exists.

In order to stabilize the mapping onto a QDM for larger values of the Josephson current, we explore alternative sets of capacitances leading to larger values for E_{hex} , more strongly suppressing non-hardcore-dimer configurations. The goal is to avoid the breakdown of the mapping before the target values for v/t —where the system is in the topological liquid phase—is reached. The dependence of E_{hex} on the capacitances C_i and C_X for two arbitrarily chosen values of C_* , obtained from a numerical second-order perturbative analysis of the ten-hexagon cluster is shown in Figs. 8(a) and 8(c). There is a region close to the C_i axis where E_{hex} peaks, the peak value increasing for smaller values of C_* .

Besides maximizing E_{hex} , we also want to optimize the amplitude t since the topological phase appears only for temperatures below the gap $\Delta \sim 0.1t$. We use second-order numerical perturbative results for the ten-hexagon cluster as a guide. For each set of capacitances we calculate the value of the Josephson current J_h giving the desired ratio $v/t = 1$, and we plot the value of t in Figs. 8(b) and 8(d). Since within perturbation theory, we are not able to determine whether a particular set of parameters leads to a valid mapping onto a QDM, we introduce an arbitrary cutoff, $J_h = E_{\text{hex}}/2$, which, based on our ENCORE results is a generous upper bound. Capacitances for which the target ratio $0.82 \lesssim v/t \leq 1$ is not reached below this bound are discarded and indicated as blank regions in the figures.

These perturbative results show that optimal values for t are obtained in a region corresponding to small val-

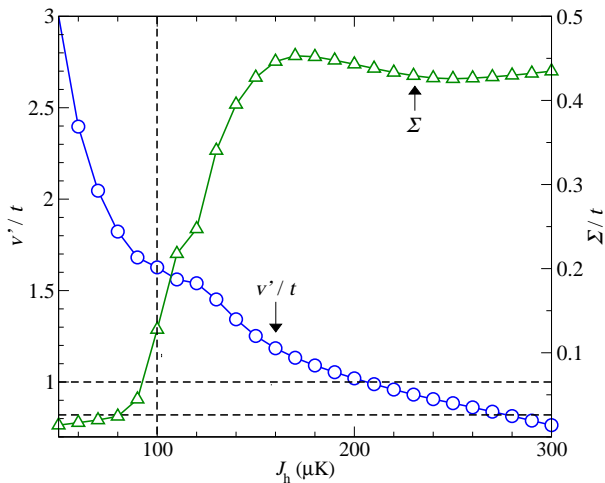


FIG. 7: (Color online) Our estimate $v' \equiv v - (u_1 - u_2)$ (circles) (Ref. 36) for the two-dimer interaction v vs the Josephson current J_h , for $C_* = C_X = 10$, $C_i = 2$ and $C_h = 0.5$, computed with ENCORE on the ten-hexagon cluster. Triangles denote the sum of the absolute values of the amplitudes (Σ) associated with *all* possible dimer moves in the ten-hexagon cluster *beyond* the lowest order ones depicted in Fig. 2(c)–2(e). The breakdown of the mapping onto a dimer model, indicated by the vertical dashed line, correlates with an abrupt increase in Σ and occurs before the topological phase of the simplest QDM for $0.82 \lesssim v/t \leq 1.0$ (indicated by the dashed horizontal lines) is reached by v'/t .

ues of C_X and close to the point where the breakdown of the mapping onto a QDM occurs before the target ratio is reached. This behavior can be understood if we analyze the dependence of $v(J_h = 0)$ and E_{hex} on C_X and C_i , shown in Figs. 6(a), Fig. 8(a), and 8(c). Since the ratio v/t decreases monotonically with J_h , larger values of $v(J_h = 0)$ have the desirable effect that values $0.82 \lesssim v/t \leq 1$ are reached for larger values of J_h , associated with more favorable values for t and Δ . Decreasing C_i at small values of C_X , we can see from Fig. 6(a) that progressively larger values of $v(J_h = 0)$ can be obtained. However, eventually, the region where E_{hex} peaks is surpassed and the mapping onto a QDM breaks down before the target ratio for v/t is reached. Decreasing C_* does virtually not affect $v(J_h = 0)$ but considerably increases E_{hex} , therefore allowing us to obtain even more favorable values for t , as shown in Fig. 8(d).

We have confirmed the validity of this qualitative analysis using ENCORE. In Fig. 9 we show v'/t as a function of J_h for two different values of C_* . For each value of C_* , C_X is chosen such that E_{hex} is close to its maximum and optimal values for t can be obtained (see Fig. 8). We terminate each curve when the mapping breaks down, as seen by nondimer intruder states in the low-energy spectrum. In Fig. 9(a) we see that for $C_* = 1$ and $C_X = 0.25$ more favorable results for t can be obtained by decreasing C_i , but below $C_i \sim 1.5$ the mapping onto a QDM breaks down before the target ratio $0.82 \lesssim v/t \leq 1$ is reached. We thus get an upper bound of $t_{\text{max}} \sim 1.5\text{mK}$

for the considered value of C_* . Larger values for the flip amplitude can be obtained if we choose *smaller* C_* . But as shown in Fig. 9(b), only slightly larger values of $t_{\text{max}} \sim 3\text{mK}$ are obtained for values of C_* two orders of magnitude smaller, suggesting that saturation is rapidly reached. Since experimentally we cannot arbitrarily decrease the ground capacitances, we conclude that we can estimate an upper-bound for the amplitude t consistent with $0.82 \lesssim v/t \leq 1$ of only a few milli-Kelvin. These optimal values are associated with small Josephson currents only slightly larger, $J_h \lesssim 10\text{mK}$, typical experimental values being close to 1K. Returning to the fact that v' underestimates v (Sec. IV B) we see that this does not influence this upper bound estimate.

Thus, even if we assume that the longer-range terms present in the emulated QDM do not destroy the topological liquid phase and that we can still estimate the topological gap as $\Delta \sim 0.1t$, we can expect that the operational temperatures for the putative quantum bit is in the micro-Kelvin regime, clearly far below the limits of current technologies.

D. Extra Flips and Interactions

So far we have ignored the presence of interactions and flips comprising three or more dimers in the effective Hamiltonian, although they are most likely relevant as suggested by the analysis of the $J_h = 0$ limit.³⁷ In Fig. 10(a) we show the dependence of the couplings on J_h for $C_* = 1$, $C_X = 0.25$, $C_i = 2$ and $C_h = 0.5$. In particular, the amplitudes associated with the unfrustrated flips involving three and four dimers [Figs. 2(d) and 2(e)] are larger than the topological gap $\Delta \sim 0.1t$ of the standard QDM. Vernay *et al.*²³ showed that the three-dimer flip extends the liquid phase. Thus, in order to be able to precisely estimate the operational temperatures for the emulated qubit, it is necessary to study the effects of the inclusion of the extra terms in the QDM. However, even in the absence of such a detailed analysis we can conclude that the involved technological challenges in reaching the sub-milli-Kelvin temperatures required for this device are substantial.

Aiming for a simpler QDM with only two- and three-dimer flips [Figs. 2(c) and 2(d)] requires the suppression of higher-order flips. We find that this requires very small values of J_h and leads to even smaller values of t . To illustrate this problem, we show in Fig. 10(b) the dependence of all couplings on J_h in the emulated QDM for $C_* = 100$, $C_X = 500$, $C_i = 10$, and $C_h = 0.5$. With $J_h = 0$ the interactions are given by $v = 0.879\text{nK}$, $u_1/v = 0.006$, $u_2/v = 0.005$, and $v' = 0.878\text{nK}$; nano-Kelvin temperatures are unrealistic in a solid-state device.

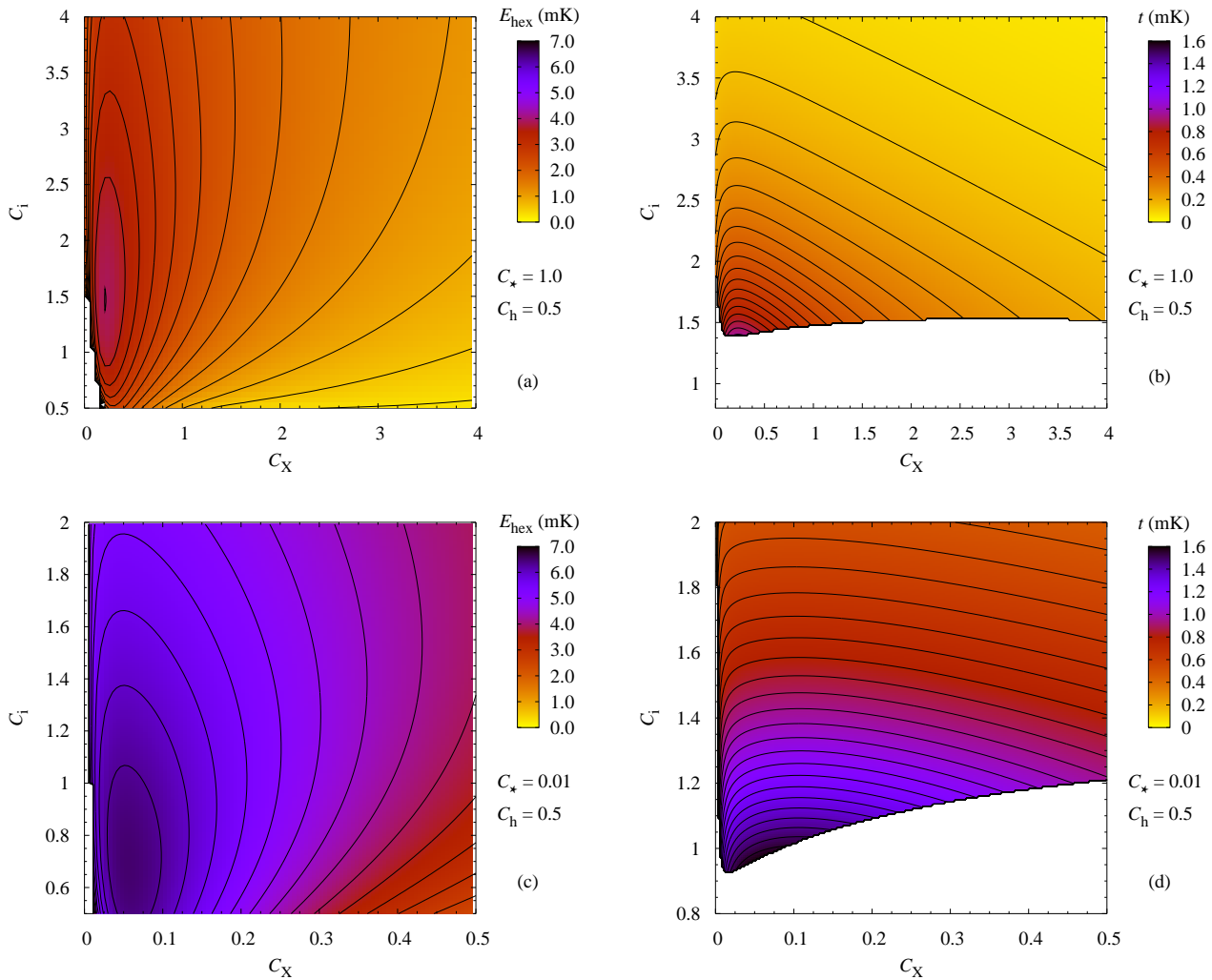


FIG. 8: (Color online) The on-hexagon repulsion E_{hex} (left panel) and the dimer flip amplitude t for $v/t = 1$, obtained by a second-order perturbative analysis of the ten-hexagon cluster, as a function of the capacitances C_X and C_i for $C_* = 1$ and 0.01 . White regions in panels (a) and (c) indicate capacitances for which E_{hex} is not a well defined quantity. In panels (b) and (d) white regions correspond to sets of parameters for which the target ratio for v/t is reached for Josephson currents $J_h \geq E_{\text{hex}}/2$, an upper bound for the largest current leading to a valid mapping onto a dimer model.

V. EMULATING QUANTUM DIMER MODELS USING COLD ATOMIC/MOLECULAR GASES

We now turn our attention to the alternative implementation based on cold atomic/molecular gases loaded into an optical lattice which was presented in Sec. II C. Since no concrete microscopic proposal is available, we restrict ourselves to order of magnitude estimates.

Flips comprising two dimers in this system similarly involve the creation of a virtual state with energy E_{\square} and thus occur, within second order in J , with amplitude $t = J^2/E_{\square}$ (we can also expect that flips involving three and four dimers may play an important role here). Since the mapping onto a QDM necessarily breaks down when the kinetic energy dominates over the on-hexagon repulsion, it follows that an upper bound for the hopping amplitude

consistent with a dimer picture is given by $J_{\text{max}} \approx E_{\square}/4$, and the largest obtainable value for the flip amplitude in such emulator is thus $t_{\text{max}} = J_{\text{max}}^2/E_{\square} \approx J_{\text{max}}/4$.

Preparation of the quantum bit state requires a controlled mixing of dimer states belonging to different topological sectors. This can be achieved by virtually breaking one dimer and creating a virtual particle-hole excitation, the particle corresponding to a doubly-occupied hexagon and the hole to an empty one.⁸ For a qubit with linear dimension corresponding to M hexagons, an upper-bound for the mixing amplitude h_x is given by

$$h_x^{\text{max}} \sim J_{\text{max}} \left(\frac{J_{\text{max}}}{2E_{\square}} \right)^{M-1} = J_{\text{max}} \left(\frac{1}{8} \right)^{M-1}. \quad (11)$$

The largest attainable experimental values for the hopping amplitude in cold atomic gases loaded into optical

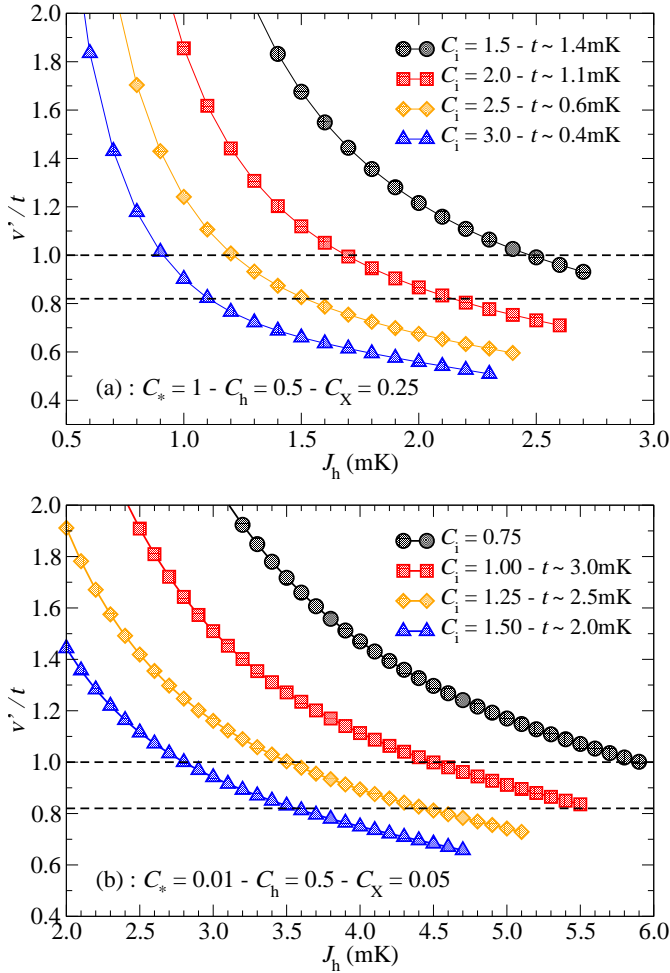


FIG. 9: (Color online) Dependence of the estimate for two-dimer repulsion v'/t on the Josephson current J_h and capacitance C_i for the ten-hexagon cluster obtained with the ENCORE algorithm for (a) $C_* = 1$, $C_X = 0.25$, and $C_h = 0.5$, and (b) $C_* = 0.01$, $C_X = 0.05$, and $C_h = 0.5$ (Ref. 37). The last data point on the right-hand side corresponds to the value of J_h for which the mapping onto a QDM breaks down. The dashed lines mark the spin-liquid phase with TQO for the standard QDM.

lattices are close to 1 kHz, smaller values being expected for more massive molecules. Thus, even on a rather small lattice comprised of the 10×10 hexagons ($M \approx 10$), we can conclude that the time-scale involved in a single qubit manipulation is of the order of minutes, much longer than typical coherence times in cold atomic gases in optical lattices.

VI. CONCLUSIONS

We have studied proposals to emulate a triangular lattice quantum dimer model (QDM). A realistic emulation of the QDM would allow the implementation of a fault-tolerant quantum bit, allowing us to circumvent the

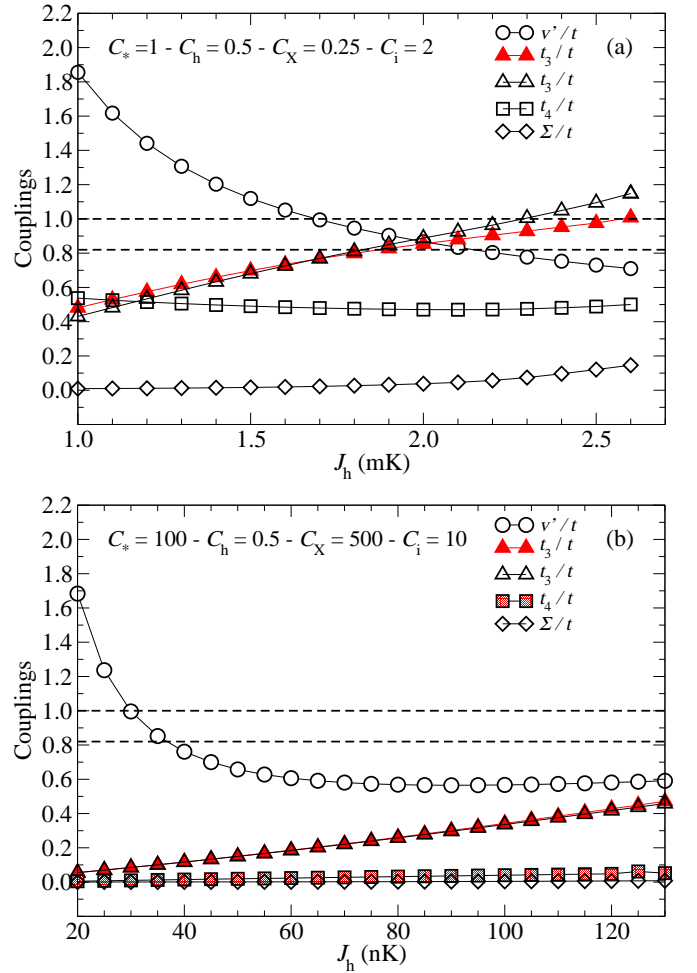


FIG. 10: (Color online) Flip amplitudes and interactions obtained by ENCORE for (a) $C_* = 1$, $C_X = 0.25$, $C_i = 2$, and $C_h = 0.5$ and (b) $C_* = 100$, $C_X = 500$, $C_i = 10$ and $C_h = 0.5$. In the upper panel only, the rightmost data point indicates the breakdown of the mapping onto a QDM. Dashed horizontal lines indicate the range of parameters corresponding to the topological phase of the standard QDM. Amplitudes for the special flips involving three (t_3) and four (t_4) dimers are also shown. For t_3 , results are obtained from the analysis of the ten (filled triangles) and six (empty triangles) hexagon clusters; t_4 is calculated from the eight-hexagon cluster. In the limit $J_h = 0$ the strengths of dimer interactions are: (a) $v = 525 \mu\text{K}$ ($v' = 390 \mu\text{K}$), $u_1/v = 0.512$, and $u_2/v = 0.253$ and (b) $v = 0.879 \text{nK}$ ($v' = 0.878 \text{nK}$), $u_1/v = 0.006$, and $u_2/v = 0.005$. Values for t corresponding to the target ratio $0.82 \lesssim v/t \leq 1.0$ are $t \sim 1 \text{mK}$ for the set in panel (a) and $t \sim 2 \text{nK}$ for the set in panel (b).

problem of decoherence which plagues more conventional proposals for achieving quantum computation.

The Josephson junction emulator by Ioffe *et al.*⁸ was studied numerically using the ENCORE method. Our results showed that the largest attainable values for the two-dimer flip amplitude t are a few milli-Kelvin and require very small Josephson currents. Since a device based on such an array would only be operational at temper-

atures considerably below the topological gap $\Delta \sim 0.1t$, implementation of a topologically-protected quantum bit with the considered array is beyond the present day technology.

The alternative array introduced by Ioffe and collaborators⁸ comprised of Y-shaped superconducting islands forming a decorated triangular lattice would lead to even lower values for the flip amplitudes since dimers in this implementation correspond to a resonating Cooper pair and dimer flips involve the tunneling of this pair through a weaker link with much smaller Josephson current. Similar challenges with too low energy scales and too long time scales are also faced by implementations using cold atomic gases.

Our results illustrate the challenges involved in the design of emulators for exotic phases. The fundamental reason for these difficulties resides in the fact that topological quantum order is a low-temperature feature, since the system's local degrees of freedom must be highly entangled over long distances, of order of the system's size, for topological order to emerge. Since emulation of the

relevant models is obtained in the low-energy limit of the proposed quantum device, we face the challenge that extremely low temperatures are required. Thus, the approach of emulating topologically ordered states for performing fault-tolerant quantum computation might only be a successful one if we can devise emulators based on much stronger bare electronic interactions, and a detailed analysis of engineering limits is required.

Acknowledgments

A.F.A. acknowledges discussions with I. Milat and the financial support from CNPq (Brazil) and NIDECO (Switzerland). H.G.K. acknowledges support from the Swiss National Science Foundation under Grant No. PP002-114713. We would like to thank A. Wallraff for the fruitful discussions. Part of the results shown in Fig. 3 were obtained by using the ALPS libraries (Refs. 38 and 39).

-
- ¹ F. Alet, A. M. Walczak, and M. P. A. Fisher, *Exotic quantum phases and phase transitions in correlated matter*, Physica A **369**, 122 (2006).
- ² L. D. Landau, Phys. Z. Sowjetunion **11**, 26 (1937).
- ³ A. Y. Kitaev, *Fault-tolerant quantum computation by anyons*, Ann. Phys. **303**, 2 (2003).
- ⁴ G. Moore and N. Read, *Nonabelions in the fractional quantum hall effect*, Nucl. Phys. B **360**, 362 (1991).
- ⁵ F. E. Camino, W. Zhou, and V. J. Goldman, *Aharonov-Bohm Superperiod in a Laughlin Quasiparticle Interferometer*, Phys. Rev. Lett. **95**, 246802 (2005).
- ⁶ D. S. Rokhsar and S. A. Kivelson, *Superconductivity and the quantum hard-core dimer gas*, Phys. Rev. Lett. **61**, 2376 (1988).
- ⁷ R. Moessner and S. L. Sondhi, *Resonating Valence Bond Phase in the Triangular Lattice Quantum Dimer Model*, Phys. Rev. Lett. **86**, 1881 (2001).
- ⁸ L. B. Ioffe, M. V. Feigel'man, A. Iosevich, D. Ivanov, M. Troyer, and G. Blatter, *Topologically protected quantum bits from Josephson junction arrays*, Nature **415**, 503 (2002).
- ⁹ G. Misguich, D. Serban, and V. Pasquier, *Quantum Dimer Model on the Kagome Lattice: Solvable Dimer-Liquid and Ising Gauge Theory in strongly correlated systems*, Phys. Rev. Lett. **89**, 137202 (2002).
- ¹⁰ L. Balents, M. P. A. Fisher, and S. M. Girvin, *Fractionalization in an easy-axis Kagome antiferromagnet*, Phys. Rev. B **65**, 224412 (2002).
- ¹¹ M. H. Freedman, C. Nayak, and K. Shtengel, *Extended Hubbard Model with Ring Exchange: A Route to a Non-Abelian Topological Phase*, Phys. Rev. Lett. **94**, 066401 (2005).
- ¹² D. N. Sheng and L. Balents, *Numerical Evidences of Fractionalization in an Easy-Axis Two-Spin Heisenberg Antiferromagnet*, Phys. Rev. Lett. **94**, 146805 (2005).
- ¹³ S. V. Isakov, Y. B. Kim, and A. Paramekanti, *Spin-Liquid Phase in a Spin-1/2 Quantum Magnet on the Kagome Lattice*, Phys. Rev. Lett. **97**, 207204 (2006).
- ¹⁴ H. Bombin and M. A. Martin-Delgado, *Topological Quantum Distillation*, Phys. Rev. Lett. **97**, 180501 (2006).
- ¹⁵ A. Kitaev, *Anyons in an exactly solved model and beyond*, Ann. Phys. **321**, 2 (2006).
- ¹⁶ H. P. Büchler, M. Hermele, S. D. Huber, M. P. A. Fisher, and P. Zoller, *Atomic quantum simulator for lattice gauge theories and ring exchange models*, Phys. Rev. Lett. **95**, 040402 (2005).
- ¹⁷ A. Micheli, G. K. Brennen, and P. Zoller, *A toolbox for lattice-spin models with polar molecules*, Nat. Phys. **2**, 341 (2006).
- ¹⁸ G. Pupillo, A. Micheli, and H. P. Büchler, *Condensed Matter Physics with Cold Polar Molecules* (2008), (arXiv:cond-mat/0805.1896).
- ¹⁹ A. F. Albuquerque, H. G. Katzgraber, and M. Troyer, *ENCORE: An Extended Contractor Renormalization algorithm* (2008), (arXiv:cond-mat/0805.2290).
- ²⁰ C. J. Morningstar and M. Weinstein, *Contractor renormalization group method: A new computational technique for lattice systems*, Phys. Rev. Lett. **73**, 1873 (1994).
- ²¹ C. J. Morningstar and M. Weinstein, *Contractor renormalization group technology and exact Hamiltonian real-space renormalization group transformations*, Phys. Rev. D **54**, 4131 (1996).
- ²² A. Ralko, M. Ferrero, F. Becca, D. Ivanov, and F. Mila, *Zero-temperature properties of the quantum dimer model on the triangular lattice*, Phys. Rev. B **71**, 224109 (2005).
- ²³ F. Vernay, A. Ralko, F. Becca, and F. Mila, *Identification of an RVB liquid phase in a quantum dimer model with competing kinetic terms*, Phys. Rev. B **74**, 054402 (2006).
- ²⁴ A. Ralko, M. Ferrero, F. Becca, D. Ivanov, and F. Mila, *Dynamics of the quantum dimer model on the triangular lattice: Soft modes and local resonating valence-bond correlations*, Phys. Rev. B **74**, 134301 (2006).
- ²⁵ P. W. Anderson, *The resonating valence bond state in La_2CuO_4 and superconductivity*, Science **235**, 1196 (1987).

- ²⁶ B. Damski, H. Fehrmann, H.-U. Everts, M. Baranov, L. Santos, and M. Lewenstein, *Quantum Gases in Trimerized Kagome Lattices*, Phys. Rev. A **72**, 053612 (2005).
- ²⁷ J. Piekarewicz and J. R. Shepard, *Plaquette basis for the study of Heisenberg ladders*, Phys. Rev. B **56**, 5366 (1997).
- ²⁸ E. Altman and A. Auerbach, *Plaquette boson-fermion model of cuprates*, Phys. Rev. B **65**, 104508 (2002).
- ²⁹ S. Capponi and D. Poilblanc, *Charge density correlations in t - J ladders investigated by the contractor-renormalization method*, Phys. Rev. B **66**, 180503 (2002).
- ³⁰ E. Berg, E. Altman, and A. Auerbach, *Singlet Excitations in Pyrochlore: A Study of Quantum Frustration*, Phys. Rev. Lett. **90**, 147204 (2003).
- ³¹ S. Capponi, A. Läuchli, and M. Mrambrini, *Numerical contractor renormalization method for quantum spin models*, Phys. Rev. B **70**, 104424 (2004).
- ³² R. Budnik and A. Auerbach, *Low-Energy Singlets in the Heisenberg Antiferromagnet on the Kagome Lattice*, Phys. Rev. Lett. **93**, 187205 (2004).
- ³³ A. Abendschein and S. Capponi, *Contractor-Renormalization approach to frustrated magnets in magnetic field* (2007), (cond-mat/0703586).
- ³⁴ We use now a value for C_* smaller than the one used in Ref. 8, since in this way it is possible to obtain larger values for E_{hex} and thus extend the mapping to larger values of J_h , as discussed in Subsection IV C.
- ³⁵ Note that for finite J_h the quality of the estimate of v improves.
- ³⁶ For the set of capacitances $C_* = C_X = 10$, $C_i = 2.0$ and $C_h = 0.5$, our estimate for the two-dimer interactions is $v' = 29.5\mu\text{K}$ when $J_h = 0$. These values should be compared with the ones obtained from the analysis of the 4×4 PBC cluster: $v = 30.6\mu\text{K}$, $u_1/v = 0.0842$ and $u_2/v = 0.0478$.
- ³⁷ For the sets of capacitances investigated in Fig. 9 the interactions in the limit $J_h = 0$, as obtained from the analysis of the 4×4 PBC, follow. (a) $C_* = 1$, $C_X = 0.25$ and $C_h = 0.5$ - (i) $C_i = 1.5$: $v = 896\mu\text{K}$ ($v' = 663\mu\text{K}$), $u_1/v = 0.476$ and $u_2/v = 0.216$; (ii) $C_i = 2.0$: $v = 525\mu\text{K}$ ($v' = 390\mu\text{K}$), $u_1/v = 0.512$ and $u_2/v = 0.253$; (iii) $C_i = 2.5$: $v = 334\mu\text{K}$ ($v' = 248\mu\text{K}$), $u_1/v = 0.539$ and $u_2/v = 0.282$; (iv) $C_i = 3.0$: $v = 226\mu\text{K}$ ($v' = 168\mu\text{K}$), $u_1/v = 0.561$ and $u_2/v = 0.304$; (b) $C_* = 0.01$, $C_X = 0.05$ and $C_h = 0.5$ - (i) $C_i = 0.75$: $v = 3.03\text{mK}$ ($v' = 1.86\text{mK}$), $u_1/v = 0.566$ and $u_2/v = 0.180$; (ii) $C_i = 1$: $v = 2.00\text{mK}$ ($v' = 1.26\text{mK}$), $u_1/v = 0.586$ and $u_2/v = 0.212$; (iii) $C_i = 1.25$: $v = 1.39\text{mK}$ ($v' = 0.89\text{mK}$), $u_1/v = 0.601$ and $u_2/v = 0.238$; (iv) $C_i = 1.5$: $v = 1.01\text{mK}$ ($v' = 0.65\text{mK}$), $u_1/v = 0.614$ and $u_2/v = 0.259$.
- ³⁸ F. Alet, P. Dayal, A. Grzesik, M. Honecker, A. Laeuchli, S. R. Manmana, I. P. McCulloch, F. Michel, R. M. Noack, G. Schmid, et al., *The ALPS project: open source software for strongly correlated systems*, J. Phys. Soc. Jap. Suppl. **74**, 30 (2005).
- ³⁹ A. F. Albuquerque, F. Alet, P. Dayal, A. Feiguin, S. Fuchs, L. Gamper, E. Gull, S. Gürtler, A. Honecker, R. Igarashi, et al., *The ALPS Project Release 1.3: Open Source Software for Strongly Correlated Systems*, J. Magn. Mater. **310**, 1187 (2007).